Shear Instability of Internal Inertia-Gravity Waves

TIMOTHY J. DUNKERTON

Northwest Research Associates, Bellevue, Washington

(Manuscript received 23 February 1996, in final form 3 December 1996)

ABSTRACT

Local shear and convective instabilities of internal inertia-gravity waves (IGW) are examined assuming a steady, plane-parallel flow with vertical profiles of horizontal velocity and static stability resembling an IGW packet in a basic state at rest, without mean vertical shear. The eigenproblem can be described in terms of a nondimensional rotation rate $R = f/\hat{\omega}_0 < 1$, where f is the Coriolis parameter, $\hat{\omega}_0$ is IGW intrinsic frequency, and IGW amplitude is a, such that $a = 1$ for convectively neutral waves. In the nonrotating case, shear instability is possible only for convectively supercritical waves, with horizontal wavevector aligned parallel or nearly parallel to the plane of IGW propagation. Transverse convection, with wavevector aligned perpendicular to the plane of IGW propagation, displays faster growth than parallel shear or convective instability at any horizontal wavenumber. For intermediate R, eigenmodes in supercritical IGW are characterized at small horizontal wavenumber k by a transverse mode of convective instability and a parallel mode of shear instability. The transverse mode again has larger growth rate at small k but is suppressed at high wavenumbers where parallel convection prevails. Shear production of perturbation kinetic energy in transverse instability is positive (negative) at intermediate or large (small) R. For R approaching unity, shear instability takes precedence over convective instability at all azimuths regardless of a. In this limit, growth of the most unstable mode is almost independent of azimuth. It is shown that the parallel shear instabilities of an IGW are analogous to the unstable modes of a stratified jet.

1. Introduction

Internal gravity waves experience amplitude growth when propagating upward in a resting, quasi-compressible atmosphere or approaching a critical level in vertical shear. As the waves grow, they become unstable to parametric instability (a resonant triad interaction at small amplitude) and shear or convective instability (a strong, local interaction). Resonant interaction may or may not be important prior to local instability, depending on how fast the waves grow. In many situations relevant to the atmosphere, it is reasonable to assume conservative wave propagation up to a ''breaking level'' where a criterion for local instability is satisfied (Lindzen 1981). This assumption simplifies matters, because no threshold for gravity wave instability actually exists.[1] The concept of wave saturation via local instability, nevertheless, has been immensely helpful for understanding the role of gravity waves in the atmosphere (Fritts 1984; Dunkerton 1989).

The general approach to gravity wave instability is via Floquet theory, a formalism for ordinary differential equations with periodic coefficients that describes the parametric instability of finite-amplitude waves (Klostermeyer 1991). This method works best at high intrinsic frequencies (Lombard 1994). Whether it is practical, or even necessary, to use Floquet theory for low-frequency waves remains to be seen. Laboratory experiments and numerical simulations of large-amplitude gravity waves display local shear or convective instabilities within the wave field (Koop and McGee 1986; Delisi and Dunkerton 1989; Winters and D'Asaro 1989, 1994; Walterscheid and Schubert 1990; Dunkerton and Robins 1992; Fritts et al. 1994; M.-P. Lelong and T. Dunkerton 1997a,b manuscripts submitted to *J. Atmos. Sci.*, hereafter LD97a,b). Eigenmodes of steady, plane-parallel flow qualitatively describe the structure and growth rate of simulated gravity wave instabilities (e.g., Dunkerton and Robins 1992). This approximation is justified if instabilities are local (compared to the horizontal scale of the gravity wave) and rapid (compared to the intrinsic timescale of the gravity wave). If these conditions are not met, or wave amplitude is subcritical with respect to local instability, the formal method is necessary.

Convective instability is relevant to nonrotating grav-

[1] Parametric instability of simple waves (without mean shear) occurs regardless of amplitude, but at small amplitude the timescale is long compared to wave period, as shown by the instability of a pendulum (McComas and Bretherton 1977). In convectively supercritical waves, transverse (convective) instabilities with large horizontal wavenumber are preferred (Klostermeyer 1991) and there is an ''isolated'' mode at low wavenumber possibly corresponding to shear instability.

Corresponding author address: Dr. Timothy J. Dunkerton, Northwest Research Associates, P.O. Box 3027, Bellevue, WA 98009.
E-mail: tim@nwra.com

ity waves in the absence of mean shear. For these waves, the local Richardson number (section 2a) is

$$\mathrm{Ri} = \frac{N^2}{(\partial U/\partial z)^2} \rightarrow 1/2 \tag{1.1}$$

at the point of isentropic or isopycnal overturning. A necessary condition for shear instability of steady, plane-parallel flow, $\mathrm{Ri} < 1/4$, is satisfied only when $\mathrm{Ri} < 0$; that is, when the waves are also convectively unstable. It is unclear which type of instability (shear or convective) will be more important in overturned waves, but the growth of convection is expected to be relatively fast if energy is initially present at large horizontal wavenumber.

In inertia-gravity waves (IGW) with constant or slowly varying amplitude, mean vertical shear ($\bar{u}_z > 0$), and/or rotation ($R = f/\hat{\omega}_0 > 0$) favor shear instability within the wave field as the primary mechanism of breakdown, because it is then possible that $0 < \mathrm{Ri} < 1/4$. For IGW without mean shear, the threshold for $\mathrm{Ri} < 1/4$ is satisfied in a direction perpendicular to the plane of IGW propagation if

$$R^{-2} < \frac{0.25a^2}{1 - a} + 1, \tag{1.2}$$

where $a = |u'/\hat{c}_0|$ is a nondimensional measure of IGW amplitude such that overturning begins at $a = 1$ (Dunkerton 1984; Fritts and Rastogi 1985). For any value of R, a larger value of a is required in order to attain $\mathrm{Ri} < 1/4$ in other azimuthal directions. It was originally thought that shear instability of IGW would appear first in the transverse direction,[2] that is, with instability wavevector perpendicular to the plane of IGW propagation, at the value of $a = a_s(R)$ implied by (1.2). In their study of shear instability in a steady, plane-parallel flow approximating that of an IGW (with no mean shear), Fritts and Yuan (1989) found, however, that significant modal instability is likely only when $R \gtrsim 0.7$. The criterion $\mathrm{Ri} < 1/4$ is evidently insufficient for modal instability in this case, nor is the depression of Ri below 1/4 by itself a good indicator of growth rate. If the concept of IGW saturation via shear instability (Dunkerton 1984) is to be useful, with threshold determined by (1.2), it must be shown (among other things) that instabilities exist in the (R, a) plane at some small distance above this threshold, with sufficiently fast growth rate to saturate, or to prevent further growth of, the primary wave. The analysis of IGW instability, however, is complicated by two factors. First, instability growth rates are relatively small near the threshold, or go to zero, so the assumption of steady, parallel flow is invalid. Eigenmodes obtained in this approximation are relevant only if their growth is rapid compared to an IGW period (Fritts and Yuan 1989). Second, the vertical structure of an inertia-gravity wave packet is approximately sinusoidal rather than having the form of a simple shear layer. As shown in section 3, the hyperbolic tangent velocity profile used by Fritts and Yuan (1989) to approximate the structure of IGW is inadequate for understanding shear instability of IGW, especially parallel modes of instability, as $R \rightarrow 1$ and/or $a > 1$.

In a slowly varying nonparallel or nonuniform flow, construction of a ''local'' instability begins with the eigenmodes of parallel flow in the complex horizontal wavenumber plane (Huerre and Monkewitz 1990; Pierrehumbert 1984; Dunkerton 1993; Clark and Haynes 1996). Local instabilities have zero group velocity with respect to the pattern of basic-state flow; in this way, their location remains fixed within, or slightly downstream from, the most unstable part of the flow. A general theory of IGW instability will benefit from the concept of ''absolute instability'' discussed in other geophysical contexts, but (as a practical matter) there is much yet to be learned about the instability of stratified shear (under the assumption of steady, parallel flow) in a configuration approximating the vertical structure of an inertia-gravity wave packet. Our understanding of eigenmodes at real $\mathbf{k}$ remains incomplete; in this paper, therefore, I consider the parallel-flow problem as a first step to a more general theory of local instability in nonuniform flow. As it turns out, unstable eigenmodes of parallel flow are useful for interpreting recent numerical simulations of breaking IGW. An immediate goal is to generalize the results of Fritts and Yuan (1989) to realistic IGW profiles and to consider a larger range of parameters (R, a) since their discussion was limited to minimum $\mathrm{Ri} = 0.10$. The stability problem is nontrivial at real $\mathbf{k}$ because different modes of instability are expected depending on IGW parameters (R, a), instability wavenumber k $(= |\mathbf{k}|)$, and orientation (α).

Section 2 reviews the theory of parallel-flow instability as applied to IGW and section 3 describes the resulting instabilities for an IGW packet without mean shear. Section 3f revisits the stability problem of Dunkerton and Robins (1992) to illustrate the effect of weak mean shear and azimuthal dependence of 3D instabilities. It will be shown that, in both prototype and ''realistic'' situations, breakdown of IGW via parallel shear instability is analogous to the instability of a stratified jet (Sutherland and Peltier 1994). The relative importance of shear and convective instability as a function of R, a, k, and α will be clarified.

2. Stability analysis

a. Theory

Instabilities on a steady, plane-parallel flow approximating a particular longitude and time of IGW motion are governed by the Taylor–Goldstein equation

[2] Mean vertical shear will tend to align shear instability in the direction of maximum total shear (Yuan and Fritts 1989).

$$\psi_{zz} + \psi\left[\frac{N^2}{(c - U)^2} + \frac{U_{zz}}{(c - U)} - k^2\right] = 0, \quad (2.1)$$

where ψ is streamfunction in the vertical plane; c and k are complex phase speed and horizontal wavenumber of instability; and N^2 and U are vertical profiles of static stability and horizontal wind in the direction of instability wavevector $\mathbf{k}$, including the IGW contribution

$$N^2 = N_0^2(1 - a\cos\Phi) \quad (2.2a)$$

$$U = a\hat{c}_0(\cos\Phi\cos\alpha + R\sin\Phi\sin\alpha) = a\hat{c}_0 U^*, \quad (2.2b)$$

where $R \equiv f/\hat{\omega}_0$, f is the Coriolis parameter, and $\hat{\omega}_0$ is IGW intrinsic frequency. The phase of IGW (Φ) is equal to $\mathbf{k}_0\cdot\mathbf{x} - \omega_0 t \rightarrow m_0 z$ in the approximation of steady, plane-parallel flow. Without loss of generality, the IGW horizontal wavevector points in the zonal (x) direction; α is the azimuthal angle between the horizontal wavevectors of IGW and instability, such that U is the component of total horizontal velocity $\mathbf{u} = (u, v)$ parallel to the instability wavevector $\mathbf{k}$,

$$U = u_{\parallel} = \mathbf{k}\cdot\mathbf{u}/|\mathbf{k}|. \quad (2.3)$$

Instabilities with $\alpha = 0°$ are referred to as ''parallel'' to the plane of IGW propagation, and instabilities with $\alpha = 90°$ as ''transverse'' to this plane. (Ordinarily, the terms ''streamwise'' and ''spanwise'' might apply, but insofar as there is no mean flow, and the IGW velocity field points in all azimuths, such usage would be ambiguous in this context.) In (2.1) it is unnecessary to know the component of horizontal velocity perpendicular to the instability wavevector, although this component may passively advect the instability wave packet. In (2.2a,b) the nondimensional amplitude of IGW is a, such that $a = 1$ at the point of overturning. For hydrostatic IGW, the intrinsic phase speed $\hat{c}_0$ is related to the vertical wavenumber m_0 through the dispersion relation

$$m_0^2 = \frac{N_0^2 k_0^2}{\hat{\omega}_0^2 - f^2} = \frac{N_0^2}{\hat{c}_0^2(1 - R^2)}. \quad (2.4a)$$

For nonhydrostatic IGW,

$$m_0^2 = \frac{N_0^2 - \hat{\omega}_0^2}{\hat{\omega}_0^2 - f^2}k_0^2 = \frac{N_0^2}{\hat{c}_0^2(1 - R^2)}\cdot\left(1 - \frac{f^2}{R^2 N_0^2}\right), \quad (2.4b)$$

which adds another parameter f/N_0 (besides R and a) to the specification of IGW basic state. Hereafter it is assumed that $f^2 \ll N_0^2$, so that the basic state is described entirely by (R, a).

Substitution of (2.2a,b) into (2.1) using (2.4a) yields the nondimensional equation

$$\psi'' + \psi\left[\frac{1 - R^2}{a^2}\frac{1 - a\cos\Phi}{(c^* - U^*)^2} + \frac{U^{*\prime\prime}}{(c^* - U^*)} - k^{*2}\right] = 0, \quad (2.5)$$

where the prime denotes differentiation with respect to nondimensional height $z^* = m_0 z$, and $k^* = k/m_0$, $c^* = c/(a\hat{c}_0)$. The static stability term is weighted by $(1 - R^2)$, so that when $R \rightarrow 1$, this term is small, and instabilities are expected to approach those of unstratified flow (Fritts and Yuan 1989). IGW amplitude appears in three ways: in the factor $(1 - R^2)/a^2$, in the phase dependence of IGW $(1 - a\cos\Phi)$, and in the dimensional form of $c = a\hat{c}_0 c^*$. Obviously, the dimensional phase speed (hence, growth rate) is proportional to a, but a also reduces the effective static stability (enhancing the growth of shear instability). When $a > 1$, convective instability is possible. The maximum growth rate of convective instability increases like $\sqrt{a - 1}$ (since the minimum N^2 decreases below zero as $1 - a$). In the following section it will be shown that, for values of $R > R_c(a)$, the growth rate of shear instability exceeds the maximum growth rate of convective instability so that shear instability takes precedence over convection even if $a > 1$. In this case, convective eigenmodes are apparently suppressed.

The azimuthal dependence is contained entirely in U, having the symmetry properties

$$U(\alpha, \Phi) = U(-\alpha, -\Phi) \quad (2.6a)$$

$$U_z(\alpha, -\Phi) = -U_z(-\alpha, \Phi), \quad (2.6b)$$

so that negation of α is equivalent to inversion of phase (i.e., the z coordinate in steady, parallel flow). When vertically symmetric boundary conditions are imposed on (2.1), it is necessary to consider only a single quadrant $0 \le \alpha \le \pi/2$. This is no longer the case when rotation is important for instability. A generalized equation for the vertical velocity perturbation, in this case, is

$$w_{zz} + w_z\left[\frac{fZ_z + f^2\hat{\omega}_z/\hat{\omega}}{\hat{\omega}^2 - f^2}\right] + w\left[\frac{(\hat{k}^2 + \hat{\ell}^2)(N^2 - \hat{\omega}^2) + \hat{\omega}(\hat{k}u_{zz} + \hat{\ell}v_{zz}) + f\hat{\omega}(Z_z/\hat{\omega})_z}{\hat{\omega}^2 - f^2}\right] = 0, \quad (2.7)$$

where $Z = i(\hat{k}v - \hat{\ell}u) = i|\mathbf{k}|u_{\perp}$, $\hat{\omega}$ is the intrinsic frequency of instability, and subscript z denotes the vertical derivative. Equation (2.6) is similar to that of Yamanaka and Tanaka (1984) for IGW in vertical

shear.[3] Hereafter the effect of rotation on instability will be ignored, that is, $\hat{\omega} \gg f$, which is satisfied if $\hat{\omega} \gg \hat{\omega}_0 \gtrsim f$ as required for the approximation of steady, plane-parallel flow to be accurate.

The profile of Richardson number corresponding to (2.2a,b) is

$$\mathrm{Ri}_\alpha = \frac{N^2}{(\partial U/\partial z)^2} = \frac{(1 - R^2)(1 - a\cos\Phi)}{a^2(R\cos\Phi\sin\alpha - \sin\Phi\cos\alpha)^2} \tag{2.8}$$

(Fritts and Yuan 1989). When $\alpha = \pi/2$, the criterion (1.2) ensures that a necessary condition for instability, $\mathrm{Ri} < 1/4$, is satisfied in the transverse direction. Larger IGW amplitudes are required for $\mathrm{Ri} < 1/4$ when $\alpha < \pi/2$. For convectively stable ($a < 1$) perturbations with horizontal wavevector in the plane of IGW propagation ($\alpha = 0$), R must exceed $\sqrt{2}/2$ for $\mathrm{Ri} < 1/4$. This condition does not guarantee the existence of unstable eigenmodes. Other factors in addition to Ri determine the growth rate (Lindzen et al. 1980). As it turns out, a clear preference for transverse eigenmodes of shear instability in convectively stable IGW exists only in a narrow range of $R \sim 0.7$–0.85 when a realistic vertical structure is assumed within the context of a steady, parallel-flow approximation. According to (1.2), there should be no critical value of $R > 0$ for shear instability in the transverse direction, but, as shown by Fritts and Yuan (1989) and in section 3, modal shear instability of convectively stable IGW is unlikely to be important when $R \lesssim 0.7$.

b. IGW configuration

The general profile of IGW adopted for this study is of the form

$$N^2 = N_0^2(1 - A\cos\Phi) \tag{2.9a}$$

$$U = A\hat{c}_0(\cos\Phi\cos\alpha + R\sin\Phi\sin\alpha), \tag{2.9b}$$

where

$$A = A(z) = a\cos^p\left(\frac{\pi z}{2z_m}\right) \tag{2.10a}$$

$$2z_m = (2n + 1)\lambda_{z0}. \tag{2.10b}$$

Here, $A(z)$ is the wavepacket envelope and λ_{z0} is the vertical wavelength of IGW. Boundaries were placed at $(-z_m, z_m)$, and the minimum static stability was located at $z = 0$. Our approach is similar to that of Fritts and Yuan (1989) but no approximation to the velocity profile was made here.

Numerical solutions of (2.1) could be obtained in a channel with rigid boundaries, radiation boundary conditions, or vertically periodic boundary conditions. Eigenmodes of interest to this study are vertically trapped away from the point of maximum instability if such a maximum exists, as guaranteed by (2.10a) if $p > 0$. For trapped disturbances, it is adequate to assume $\psi' = 0$ at the boundaries if they are placed far enough away from the center of eigenfunction.

Two sets of experiments demonstrated the effect of configuration parameters (n, p) on the solution. In one set, boundaries were moved progressively farther away, holding the wave packet envelope approximately constant (increasing n and p simultaneously). In another set, boundaries were moved farther away, allowing the wave packet to fill the channel (increasing n, holding $p = 1$). The first set of experiments showed that at least three vertical wavelengths ($n = 1$) were necessary to obtain eigenfunctions decaying exponentially at the boundaries; convergence was obtained with five or more wavelengths ($n \geq 2$). The second set demonstrated how local eigenfunctions obtained in (2.9) gradually evolve into periodic solutions as the vertical extent of the wave packet increases.

It is impossible to analyze all IGW configurations, so it is assumed hereafter that (n, p) = (3, 1). This combination maximizes vertical resolution of the IGW profile for a fixed number of gridpoints while ensuring that boundaries have a negligible effect on the eigenmodes of interest. Two solution methods were employed, similar to those of Dunkerton (1990): (i) a shooting technique for complex eigenfrequency $\hat{\omega}$ enabled all modes to be obtained regardless of growth rate and (ii) an implicit time-dependent code gave the most unstable mode at each k. For the most unstable mode, nearly identical results were obtained with the two methods. In the time-dependent technique, the equations of motion are

$$D_t u' + w'U_z + p'_x = 0, \tag{2.11a}$$

$$D_t w' + p'_z - b' = 0, \tag{2.11b}$$

$$D_t b' + N^2 w' = 0, \tag{2.11c}$$

$$u'_x + w'_z = 0, \tag{2.11d}$$

where u', w' now represent horizontal and vertical velocity perturbations; p' is the pressure perturbation normalized by basic density; b' is the buoyancy perturbation; and

$$D_t = \frac{\partial}{\partial t} + U\frac{\partial}{\partial x}. \tag{2.12}$$

where [in (2.11) and (2.12) only] x points in the direction of instability wavevector. Disturbances are incompressible, nonrotating, and nonhydrostatic. Time derivatives are written in finite-difference form; for example, as

$$\frac{\partial u}{\partial t} = \frac{u_{n+1} - u_n}{\Delta t} = \frac{2}{\Delta t}(\hat{u} - u_n), \tag{2.13}$$

where $\hat{u}$ is evaluated midway between two adjacent time steps. The relevant Taylor–Goldstein equation is then

[3] Minor differences arise due to their assumption of geostrophically balanced basic state, as opposed to unbalanced IGW.

$$\hat{\psi}_{zz} + \hat{\psi}\left[\frac{N^2}{(c - U)^2} + \frac{U_{zz}}{(c - U)} - k^2\right] = \mathcal{D}, \quad (2.14)$$

where $c = 2i/k\Delta t$ and $\mathcal{D}$ is a complicated expression involving fields at the nth time step. The tridiagonal algorithm was used to solve this equation as in (2.1), with 201 vertical grid points.

3. Instability of a wavepacket

For any IGW configuration (n, p) the instability is a function of nondimensional rotation rate $R = f/\hat{\omega}_0$, IGW amplitude a, instability horizontal wavenumber k, and orientation α relative to the horizontal component of inertia-gravity wavevector. At small to intermediate R, local instability is significant only for convectively supercritical IGW ($a > 1$). At large R ($\lesssim 1$), instability is important for subcritical as well as supercritical a. To simplify the investigation, a convectively supercritical case ($a = 1.5$) was examined for $0 \leq R \leq 0.95$ over a range of k and several horizontal azimuths α. For eigenmodes with *local* maximum growth rate at some real $k = k_m$, the variation of maximum growth rate as a function of R, a, or α was determined by varying these parameters gradually while varying k at the same time, such that $k = k_m(R, a, \alpha)$. It is important to remember that, depending on the behavior of convection at large k, such a local maximum does not necessarily represent the most unstable wavenumber over all k.

a. Supercritical a, R = 0

When $R = 0$, there is no transverse velocity component of the IGW. As shown in Fig. 1, the preferred instability is transverse ($\alpha = 90°$) without horizontal scale selection. Growth rate asymptotes to the maximum growth rate of convection $N_0\sqrt{a - 1}$ as $k \to \infty$. The instability is purely convective. Results at $\alpha = 60°$ are similar, with slightly lower growth rate at any k. In the zonal direction ($\alpha = 0°$), there is a local maximum at small k representing the so-called radiating mode of shear instability (Dunkerton and Robins 1992, hereafter DR). This peak is slightly larger and less distinct at $\alpha = 30°$. All azimuths display convective instability at large k.

Structure of the parallel mode of shear instability at $k = k_m \approx 1.6 \times 10^{-3}$ m^{-1} is shown in Fig. 2a. The IGW velocity profile in this direction is shown in Fig. 2b, with instability critical levels superposed. These levels are adjacent to local minima of the eigenfunction. There are two critical levels on either side of the jet maximum and three primary lobes of streamfunction amplitude. The eigenfunction decays rapidly to zero before encountering the boundaries. Phase lines appear to radiate away from center. In physical space, isopleths of phase are tilted against the mean shear, making the shear a source of perturbation kinetic energy (PKE) as in DR. Those authors referred to the parallel eigenmode as a radiating mode of convective instability aided by shear generation of PKE. This interpretation is misleading and should be changed to indicate an eigenmode of shear instability (hereafter S_1) with phase tilt aligned against the mean shear. Negative static stability is not essential to the growth of this mode, as shown below.

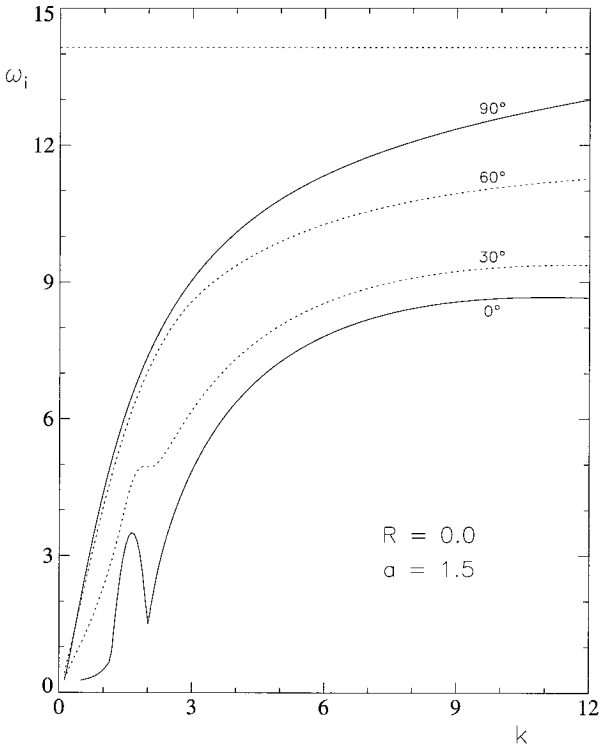

FIG. 1. Growth rate of IGW instabilities with horizontal wavevector in the parallel ($\alpha = 0°$, lower solid curve) and transverse direction ($\alpha = 90°$, upper solid curve) for (R, a) = (0.0, 1.5) obtained from the time-dependent model, showing the most unstable mode as a function of k. Two intermediate azimuths are also shown ($\alpha = 30°$, 60°, dotted lines). In this figure and the following, dimensional growth rates and wavenumbers are indicated (multiplied by 1000) for basic-state parameters $N_0^2 = 4 \times 10^{-4}$ s^{-2} and $\hat{c}_0 = 10$ m s^{-1}. Horizontal dotted line at top displays the maximum growth rate of convective instability as $k \to \infty$.

Growth rate at $\alpha = 0°$, $k = k_m$ is less than that of other azimuths, so it will be difficult to excite the parallel mode in a 3D simulation (even if the initial noise falls off rapidly with k) unless there is substantially more energy in the zonal direction than in other azimuths. This situation could arise if the spectrum at early times is due entirely to self-interaction of the primary wave (as in DR).

b. Supercritical a, intermediate R

As R is increased above zero, a meridional velocity component of IGW appears in quadrature with the zonal component, with relative magnitude R. The vertical wavelength of IGW diminishes slowly as $\sqrt{1 - R^2}$. For parallel instability ($\alpha = 0°$), the meridional velocity

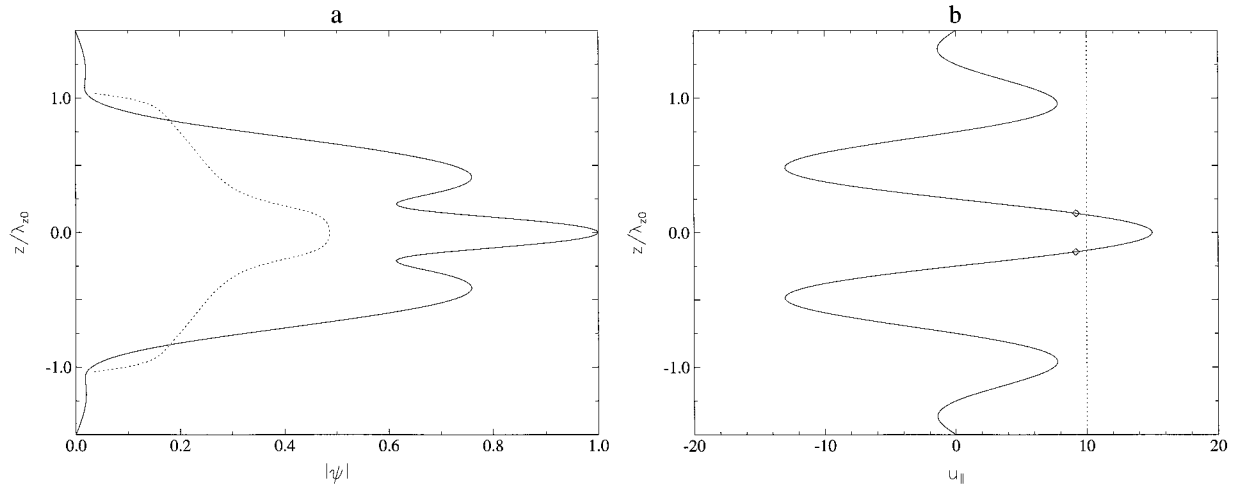

FIG. 2. (a) Streamfunction amplitude (solid) and phase (dotted), and (b) IGW velocity profile, for S_1 mode at $\alpha = 0°$, $k = k_m \approx 1.6 \times 10^{-3}$ m^{-1} when $(R, a) = (0.0, 1.5)$. Phase of ψ on the x axis extends from $-\pi$ to π. In physical space, isopleths of phase are oppositely tilted. Instability critical levels are indicated by diamonds in (b).

component does not enter the eigenproblem and therefore has no direct effect on growth rate. As shown in Fig. 3 for $R = 0.6$, parallel instabilities experience a small reduction of growth rate at all k and a shift of the S_1 peak to slightly higher k. Growth rates are plotted versus dimensional k in these figures; the shift to higher k is consistent with a slight reduction of λ_{z0}. In marked contrast, the transverse instability ($\alpha = 90°$) at large k is suppressed by transverse velocity shear due to small or moderate R. Note that IGW vertical shear *within the region of overturning* maximizes in the transverse direction. The transverse mode persists at small horizontal wavenumber and remains the most unstable azimuth at small k, as it was for $R = 0$. At $\alpha = 30°$, growth rates for large k are now slightly smaller than at $\alpha = 0°$. At $\alpha = 60°$, growth rates for small (large) k are less than (greater than) those at $\alpha = 90°$.

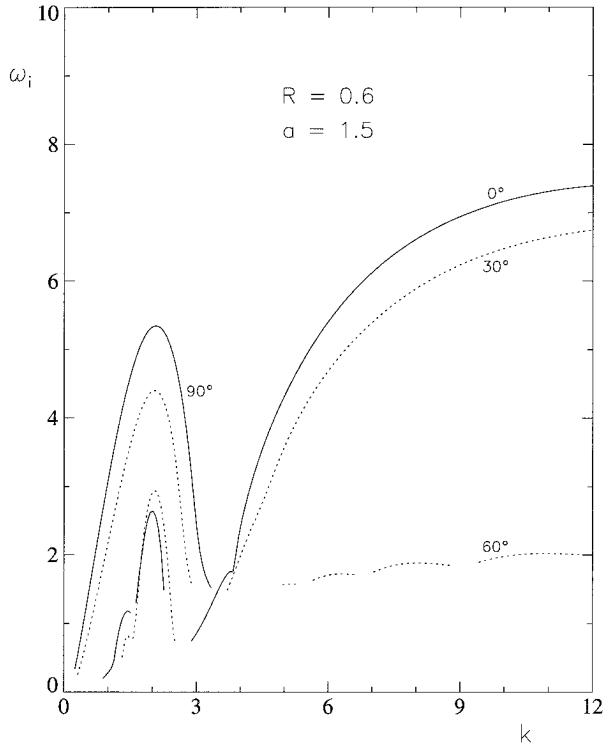

FIG. 3. Growth rate as in Fig. 1, but for $(R, a) = (0.6, 1.5)$.

For intermediate R, transverse instability is preferred at small horizontal wavenumber while parallel instability is preferred at large horizontal wavenumber. In numerical simulations, the transverse instability will assume greater importance if hyperdiffusion suppresses the motion at large k and/or there is substantially more energy initially available at small k.

Structure of the transverse eigenmode at $k = k_m \approx 2.1 \times 10^{-3}$ m^{-1} for $R = 0.6$ is shown in Fig. 4, together with the IGW velocity profile in this direction. The eigenfunction has a single peak at the center of the region of overturning. On either side, phase lines in physical space tilt against the mean shear, so that shear generation of PKE is positive. Mean shear evidently broadens the eigenfunction (relative to that of purely convective modes), giving it something of a triangular shape. The interpretation of this mode is that of a convective instability, or hybrid shear–convective instability, significantly enhanced by shear generation of PKE, with scale selection attributable to the transverse shear.

As R is reduced back to zero, $k_m \to \infty$ at $\alpha = 90°$ and the transverse eigenmodes become essentially convective. Unlike the situation for $R = 0.6$ (Fig. 4a), convective modes for $0 < R \lesssim 0.4$ have modest phase tilt aligned *with* the mean shear within the region of overturning so that shear generation of PKE is evidently negative; that is, transverse mean shear is a sink of PKE.

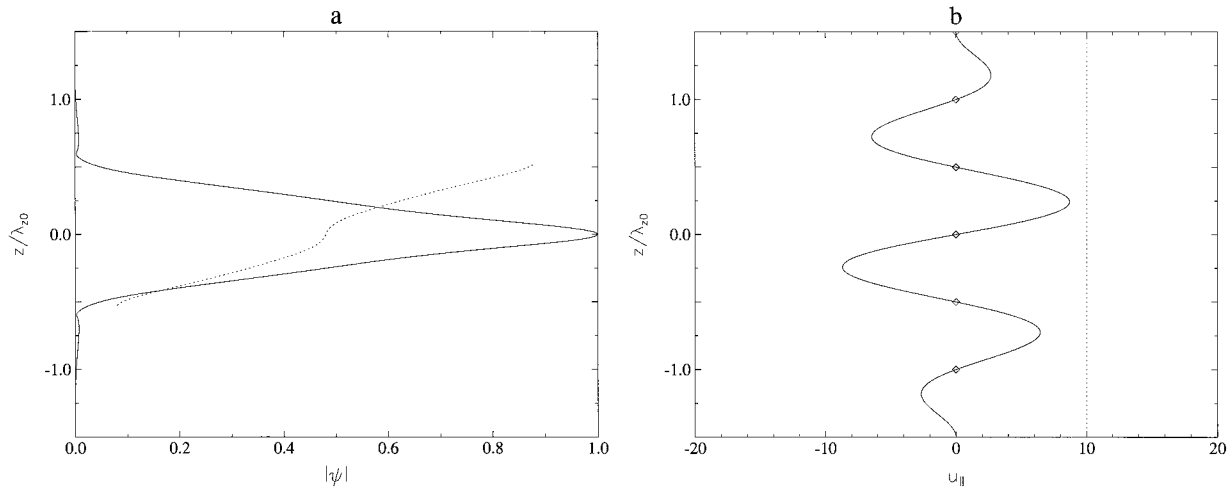

FIG. 4. Streamfunction and IGW velocity profile as in Fig. 2, but for transverse eigenmode $\alpha = 90°$, $k = k_m \approx 2.1 \times 10^{-3}$ m^{-1} when (R, a) = (0.6, 1.5).

This result is consistent with recent numerical simulations of convectively supercritical IGW by D. C. Fritts (1995, personal communication).

c. $R \lesssim 1$

When R approaches unity, convective eigenmodes are suppressed within the range of k that was investigated; shear instabilities dominate. Remarkably, growth of the S_1 mode depends only weakly on azimuth, as shown in Fig. 5. A second mode (S_2) appears at small k, to the left of the kink in Fig. 5, with antisymmetric streamfunction about the center. The two modes S_1, S_2 may be likened to the sinuous and varicose modes of the stratified Bickley jet, respectively (Hazel 1972). Trajectories of complex $\hat{\omega}(k)$ for S_1 and S_2 are nonintersecting; the S_2 mode has a much larger phase speed and greater sensitivity to azimuth α. Near its peak growth rate, the S_1 mode exceeds the maximum growth rate of convection (horizontal dotted line).

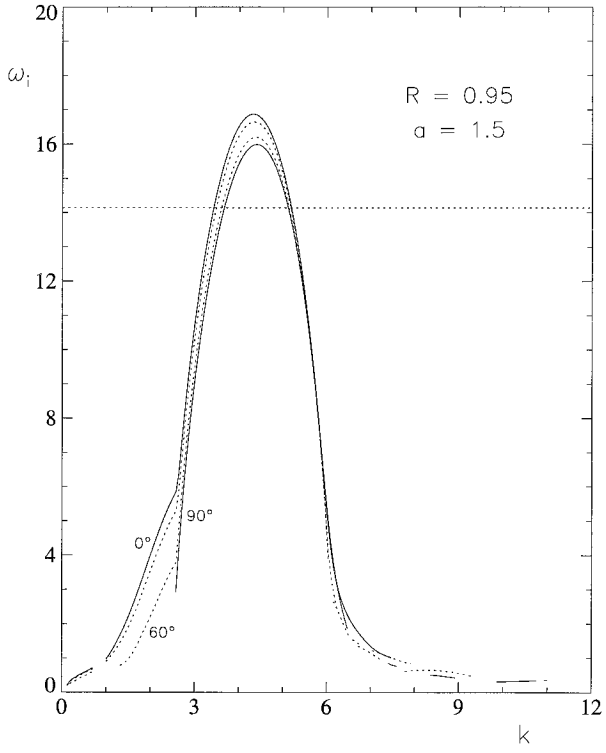

FIG. 5. Growth rate as in Fig. 1, but for (R, a) = (0.95, 1.5).

Structure of the parallel ($\alpha = 0°$) eigenmode at $k = k_m \approx 4.3 \times 10^{-3}$ m^{-1} is shown in Fig. 6, together with the IGW velocity profile and instability critical levels. This mode is similar to the $R = 0$ version of S_1 (Fig. 2a) but has much slower phase speed and several critical levels. The phase function oscillates vertically in tandem with U. In physical space, the instability's phase tilt opposes the mean vertical shear throughout the IGW field. The instability, as it were, is extracting kinetic energy from the IGW in an optimum way. When α is varied, the eigenmode shifts upward roughly by a distance α, so that when $\alpha = 90°$, this mode has two maxima straddling a local minimum at $z = 0$ (not shown). Growth rate is approximately independent of α because the ''wave geometry'' (Lindzen et al. 1980) is relatively constant, thanks to the nearly helical velocity profile of IGW and small phase speeds of instability. In other words, the IGW velocity component $u_\parallel$, position of instability critical levels z_c, and values of (1/4 − Ri) at the critical levels are similar except for the velocity profiles and critical levels being translated upward by a distance proportional to α. Recent 3D numerical simulations of large-amplitude IGW by LD97a,b in a triply periodic domain also demonstrate that the growth rate and most unstable wavenumber of the sinuous mode are insensitive to α.

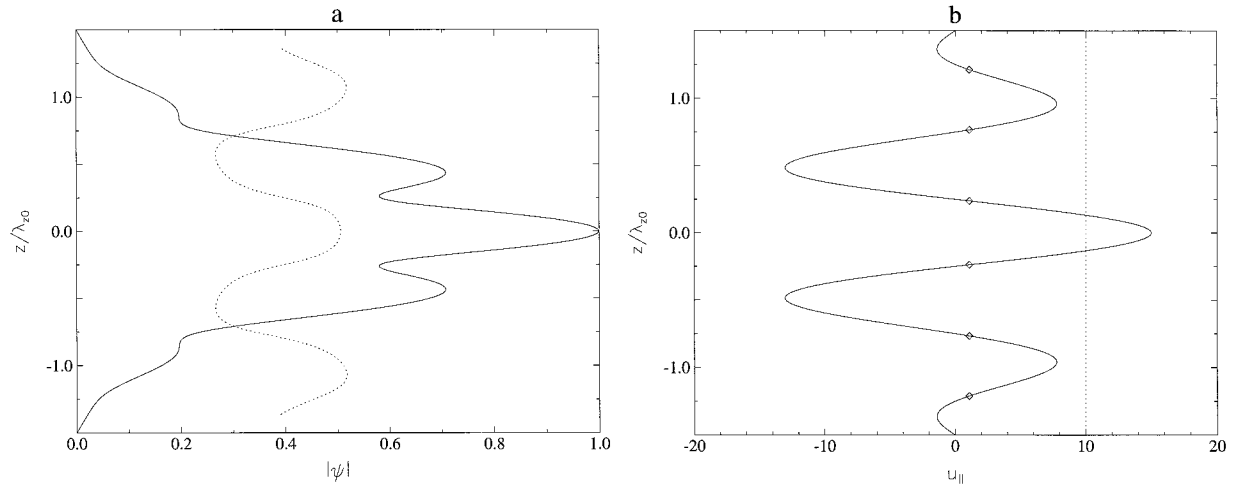

FIG. 6. Streamfunction and IGW velocity profile as in Fig. 2, for S_1 mode at $\alpha = 0°$, $k = k_m \approx 4.3 \cdot 10^{-3}$ m^{-1} when $(R, a) = (0.95, 1.5)$.

d. Local maximum ω_i

Figure 7 shows the local maximum growth rate at $k = k_m$ for transverse ($\alpha = 90°$) instability as R varies from 0 to 0.95, for several values of $a = 0.9$–1.5. An example of parallel ($\alpha = 0°$) instability is also shown for $a = 1.5$ (dash–dot line). For the parallel S_1 mode, if $R \lesssim 0.85$, this is *not* the most unstable wavenumber over all k because parallel convection has larger growth rate (cf. Figs. 1 and 3). It is interesting, nonetheless, that a parallel mode of shear instability exists throughout the range of R if $a \gtrsim 1.3$. For transverse instability (solid lines), growth rate is minimum at intermediate R and climbs steadily as $R \to 0$, approaching the maximum growth rate of convection where $k_m \to \infty$. (This is indicated by dashed lines because the numerical calculation does not extend to infinite k.) Curves at $\alpha = 60°$ (not shown) terminate prior to $R = 0$ when a finite k_m ceases to exist. Transverse modes have significantly larger growth rates than parallel modes when $R \lesssim 0.85$, while for larger R there is a weak preference for parallel modes. Horizontal wavenumbers k_m (not shown) are larger in the transverse direction and display a similar variation with R as that of ω_i.

At large R, for any value of a, the growth rate of shear instability exceeds the maximum growth rate of convection. The two are equal along a curve $R = R_c(a)$ that can be visualized by connecting the locus of points where, for each a, the growth rate of shear instability intersects the corresponding horizontal (dotted) line. Values of R_c are approximately 0.92–0.95 in the range $a = 1.1$–1.5.

As a is reduced below 1.5, modal growth rates diminish to zero approaching a neutral curve $a = a_n(R, \alpha)$. Resolvable modal growth begins near $a = 1$ for small and intermediate R. Even at $(R, a) = (0.7, 1)$ the modal growth rate is very small (~ 0.00024 s^{-1}). A transverse eigenmode is found at this point, containing maximum $|\psi|$ at the location of maximum transverse velocity shear, with phase tilted against the shear (not shown). The IGW is convectively neutral; therefore shear production of PKE is the exclusive mechanism of generation. Only in the range $0.7 \lesssim R \lesssim 0.85$ and $a \lesssim 1$ is there a clear preference for transverse eigenmodes of shear instability in the steady, parallel-flow approximation. For supercritical a in this range of R, transverse modes are preferred but are driven by a mixture of buoyancy and shear effects. At $R = 0.95$, transverse modes have slightly larger growth rates than parallel modes in the range $0.75 \lesssim a \lesssim 0.90$, while parallel modes have slightly larger growth rates for values of a outside this range. These differences are insignificant from a modeling point of view (LD97a). Structure of the eigenmodes at $R = 0.95$ is similar for subcritical and supercritical values of a.

e. Interpretation

The weak azimuthal dependence of shear instability at large R is unexpected from earlier results of Fritts and Yuan (1989), which show a clear preference for transverse instability. Interpretation of the parallel instability (S_1) as a symmetric mode of an unstable jet is evidently important to this weak α dependence. A jet structure in the zonal direction implies two instability critical levels situated symmetrically about the jet maximum. When a hyperbolic tangent profile is used to approximate the velocity structure of IGW (Fritts and Yuan 1989), there is at most one instability critical level. An unstable parallel mode exists in their geometry but is displaced away from the static stability minimum (where the transverse mode is centered). Here $\mathrm{Ri}(z_c)$ is lowest in the transverse direction in their profile as well as ours, but in IGW the zonal direction has two equal (though slightly larger) values of $\mathrm{Ri}(z_c)$ that, in combination, produce a parallel shear instability that is competitive with transverse instability.

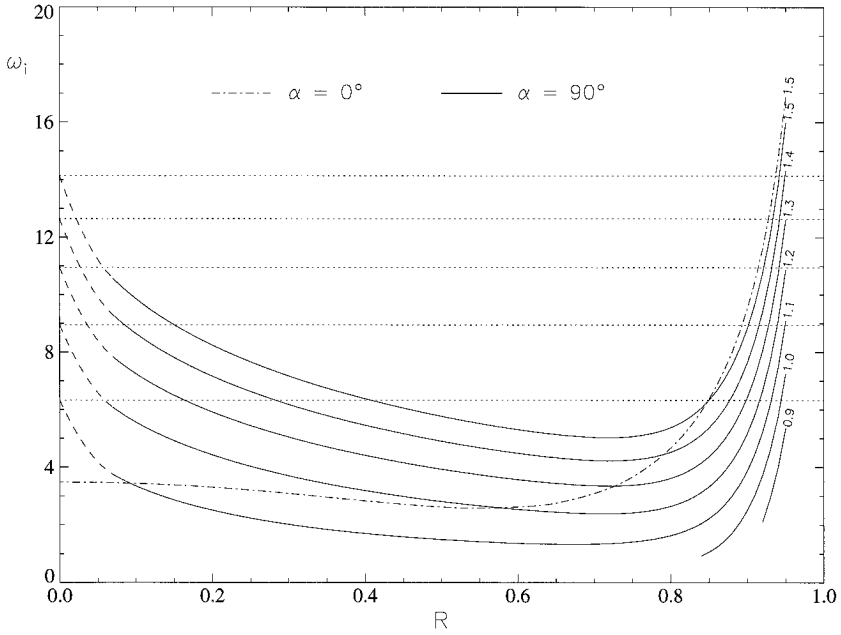

FIG. 7. Growth rate of transverse instability at $k = k_m$ for several values of a (solid lines) as a function of R. An example of parallel shear instability is also shown for $a = 1.5$ (dash–dot line). Horizontal dotted lines indicate the maximum growth rate of convection at $a = 1.1$, 1.2, . . . , 1.5.

Two variations of IGW velocity profile were examined to clarify the role of twin critical levels at $\alpha = 0°$. In the first variation, the zonal velocity component was set to its minimum value outside the central lobe of the IGW, preserving the exact jet structure in the center of the channel and continuity of U, U_z at $z = \pm\lambda_{0z}/2$. This modification resulted in a parallel eigenmode with slightly lower horizontal wavenumber k_m and approximately the same growth rate as before. Amplitude and phase of the eigenfunction are shown in Fig. 8a and the modified velocity profile is shown in Fig. 8b. Phase tilts are confined to the flanks of the jet, but the structure is otherwise similar to that of Fig. 6a. A varicose mode also exists in this profile. In the second variation, the zonal velocity component was truncated to a quarter (rather than half) wavelength, producing a single shear layer. This gave a more substantial reduction of k_m to about two-thirds of its unaltered value and reduction of ω_i by about 15%. Structure of the eigenfunction (Fig. 9a) was similar to that of a transverse mode except for being shifted off center. Only a single critical level exists (Fig. 9b). The domain in this case was barely tall enough

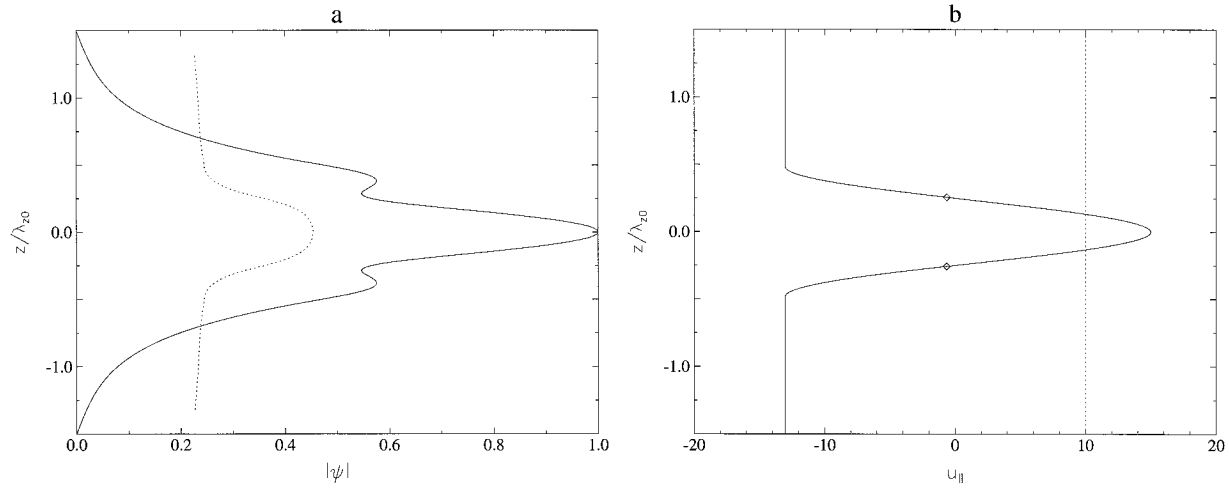

FIG. 8. Streamfunction and IGW velocity profile for parallel mode of Fig. 6, but with modified velocity profile (jet structure).

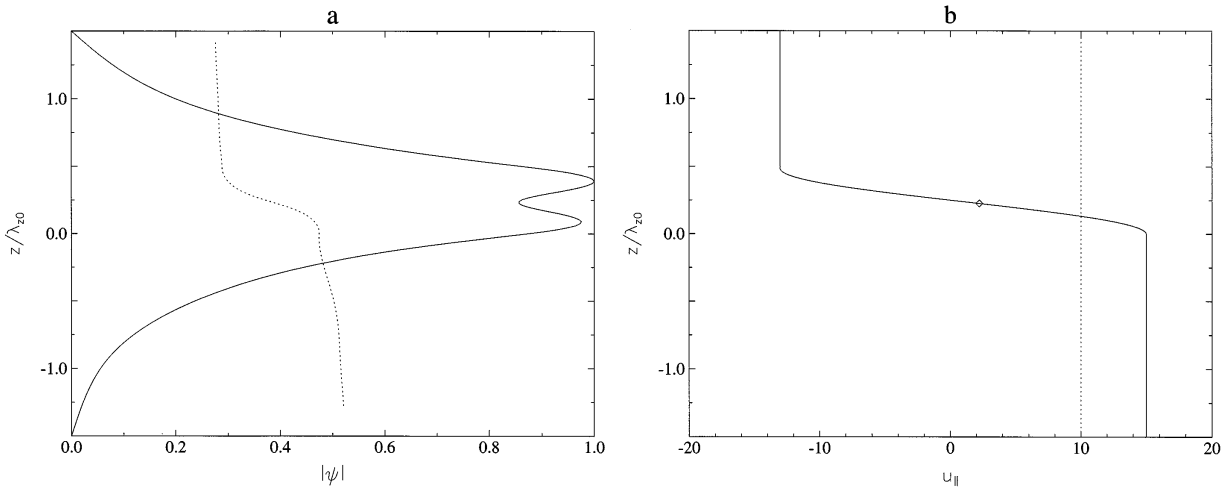

FIG. 9. Streamfunction and IGW velocity profile for parallel mode of Fig. 6, but with modified velocity profile (single shear layer).

to contain the eigenfunction, but similar results were obtained at larger n, with larger reduction of ω_i. From this example it is clear that the hyperbolic tangent approximation reduces the growth rate of the parallel mode.

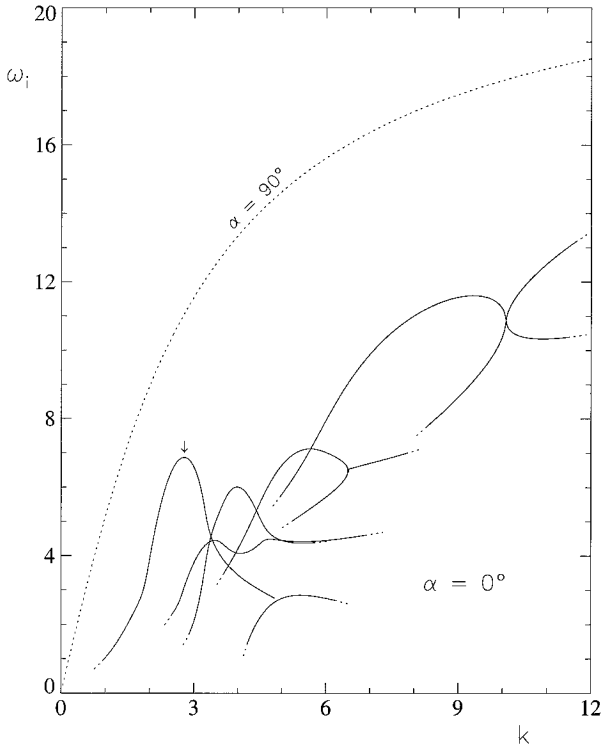

FIG. 10. Growth rate of parallel ($\alpha = 0°$) instabilities, obtained with the shooting method, in the example of Dunkerton and Robins (1992, their Fig. 9) in which a nonrotating gravity wave approaches a critical level in vertical shear. Transverse convection ($\alpha = 90°$) is shown by the upper dotted line. An arrow indicates the dominant mode of parallel shear instability identified previously.

Growth of transverse modes, on the other hand, was rather unaffected by this variation (when applied to the meridional velocity component v). The hyperbolic tangent approximation is evidently able to reproduce the growth rate, but not vertical structure, of transverse instabilities fairly well. As a is reduced in the truncated velocity profile, the disparity between parallel and transverse eigenfrequencies is expected to increase, because $\mathrm{Ri}(z_c) \rightarrow 1/4$ in the zonal direction prior to $\mathrm{Ri}(z_c) \rightarrow 1/4$ in the meridional direction.

f. Effect of mean shear

Two-dimensional numerical simulations of a gravity wave critical layer by DR showed that a mode of shear instability developed prior to convection. Eigenmodes of parallel flow explained the existence and scale selection of this mode reasonably well. The question remains as to what instability orientation (e.g., parallel or transverse) would be most important in a 3D simulation. Results of section 3a suggest that transverse convection will dominate at all horizontal wavenumbers. Figure 10 displays an updated calculation of the growth rate of parallel and transverse instabilities in DR's wave packet, without mean flow modification (refer to their Fig. 9 for $\bar{u}$ and $\bar{\theta}$ profiles). Eigenfrequency trajectories (obtained with the shooting technique) are more complicated than anticipated by DR. The dominant mode of parallel convection at large k grows faster than shown in Fig. 10 of DR and agrees much better with their time-dependent numerical results. Additional modes appear at intermediate wavenumbers that provide a better explanation of multiple spectral peaks in DR's simulations. Time-dependent calculations (not shown) confirm the existence of three peaks at small and intermediate k, below the convective continuum at large k.

The most important observation in Fig. 10 is that the

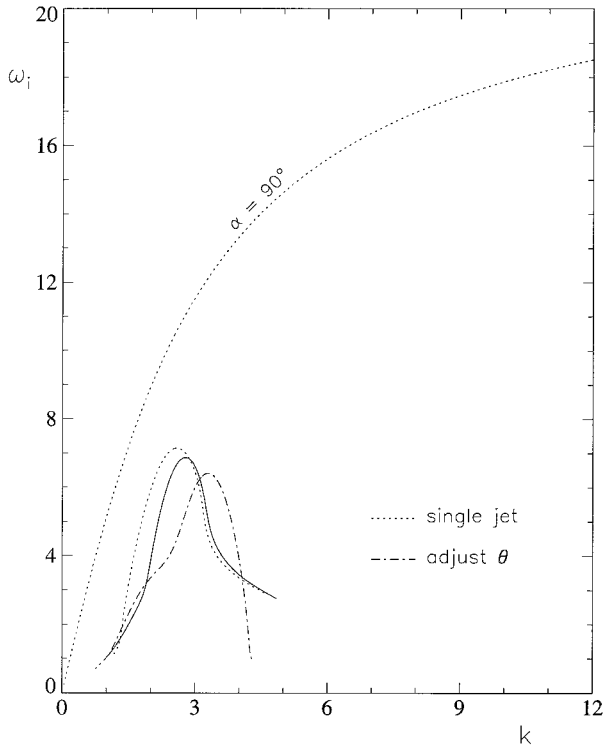

FIG. 11. Growth rate of parallel instability as in Fig. 10 (small-*k* lobe only) after convective adjustment was applied to the potential temperature profile (dash–dot line). The effect of modifying the velocity profile, retaining only a single jet at the center of the wave packet, is shown by the dotted line.

growth of parallel eigenmodes is dwarfed by transverse convection ($\alpha = 90°$). In a 3D simulation, therefore, transverse convection will overtake parallel shear instability if isotropic noise is initially present. Conceivably, parallel shear instabilities might develop first if the initial wavenumber spectrum is due entirely to self-interaction of the primary wave. This would require a ''clean'' background state devoid of waves or turbulence in other azimuths, an unlikely situation in reality. The role of mean flow modification is to enhance the growth of parallel shear instability as demonstrated in the appendix of DR.

Figure 11 illustrates the parallel eigenmode's growth rate (showing the lobe at small *k* only) after convective adjustment was applied to the potential temperature $\bar{\theta}$ profile, leaving the velocity profile unaltered. Growth of the shear instability is shifted to a slightly higher wavenumber but not significantly attenuated. Convection is now absent in all azimuths, and only shear instability remains, with maximum growth rate in the zonal direction. The absence of convection was confirmed using the time-dependent code. Shear instability is therefore possible in a convectively adjusted gravity wave critical layer. The effect of turbulence produced by convection is not taken into account, however, nor is any change in the velocity profile. Figure 11 also shows the effect of modifying the velocity profile such that only a single jet remains at the center of the wave packet (without any adjustment to $\bar{\theta}$). In agreement with the previous section, the eigenfunction and growth rate are insensitive to the flow outside this region.

4. Discussion

The preceding theoretical analysis demonstrates that shear instability of internal gravity waves is important in several circumstances. 1) If the initial noise spectrum is biased in the direction of the primary wave (e.g., due to self-interaction), shear instability will develop after overturning (Dunkerton and Robins 1992). Parallel shear instability may coexist with transverse convection (or develop as a result of shear enhancement due to convection) as shown by Fritts et al. (1994) and Winters and Riley (1992). 2) If $R = f/\hat{\omega}_0$ approaches unity prior to overturning, shear instability is the primary mechanism of breakdown (Dunkerton 1984; Fritts and Rastogi 1985; Fritts and Yuan 1989). 3) If, for some reason, the IGW packet evolves toward supercritical *a* too rapidly for shear instability to develop at subcritical *a*, shear instability will nevertheless dominate at supercritical *a* for values of $R > R_c(a)$. Without mean vertical shear, little azimuthal preference is likely at large *R* regardless of *a*. 4) For intermediate *R*, transverse modes of mixed convective–shear instability occur in supercritical IGW. 5) Shear instability is enhanced by formation of a ledge at the base of the critical layer when mean flow modification occurs (Dunkerton 1982; DR).

Numerical simulations by DR and Fritts et al. (1994) and laboratory experiments of Delisi and Dunkerton (1989) contained a mean vertical shear in addition to the local shear attributable to the gravity wave. Mean shear unfortunately adds another variable to an already overcrowded IGW parameter space (n, p, R, a, k, α), so an analysis of its influence is beyond the scope of this paper. Nevertheless, it is important to distinguish two effects of mean vertical shear on gravity wave breakdown. First, mean shear superposes on that of the wave, at certain phases constructively, so that shear instabilities tend to align in the direction of the (wave + mean) shear (Yuan and Fritts 1989). Second, the primary wave may encounter a critical level in mean vertical shear (if such a level exists), resulting in rapid amplification of u_z'. In DR, the second effect was more important than the first. The nature of this amplification is to produce a jetlike structure of $(\bar{u} + u')$ beneath the critical level, coincident with a local minimum of static stability. For inertia-gravity waves [ignoring the subtleties of a valve effect discussed by Yamanaka and Tanaka (1984)] growth of a helical velocity structure is expected, with similar amplification of vertical shear but in all azimuths. In a complicated field of small-amplitude IGW dominated by critical-layer interactions, one can imagine the apparently spontaneous formation of these jets (or helixes) accompanied by local shear or

convective instabilities and patches of turbulence (Barat 1983).

The instability of a stratified jet is relevant to zonally aligned shear instabilities at any R. Eigenmodes are characterized by amplitude and phase variations that are vertically coupled so as to eventually lead to the formation of staggered Kelvin–Helmholtz billows on opposite sides of the jet maximum (LD97a). This situation is analogous to that of Sutherland and Peltier (1994), who show the effects of stratification on the finite-amplitude evolution of instabilities in a Bickley jet. The unstratified case generates staggered vortices of opposite sign on either side of the jet, whereas in stratified flow the overturning of isopycnals leads to turbulent breakdown and mixing. While our attention in this paper has focused entirely on the theoretical aspects of linear eigenmodes, it is the turbulent breakdown, momentum deposition, and mixing attributable to the growth of instability that is ultimately of interest. The mixing efficiency of breaking IGW has not been addressed in the literature, except in nonrotating waves (Fritts and Dunkerton 1985; Coy and Fritts 1988). Little is known about the role of inertia-gravity waves in vertical mixing of the atmosphere and ocean.

Two limitations of the theoretical analysis are 1) the approximation of steady, plane-parallel flow to represent IGW motion, and 2) the assumption that eigenmodes, growing from small background noise, are relevant. The analysis can be extended to complex horizontal wavenumber to examine absolute instability, retaining the assumption of steady flow in a frame of reference translating with the phase speed of IGW. The criterion for absolute instability in this context is that modes exist with group velocity identical to the zonal phase propagation of a background IGW. Differences between ''convective'' and ''absolute'' instability usually involve a slight reduction of growth rate and change of horizontal scale with respect to $k = k_m$. Further theoretical analysis, to be reported separately, indicates that a saddle point exists in the complex zonal wavenumber plane for azimuths extending from 0° to about 45°. Numerical results of LD97a demonstrate that instability wave packets evolve during their linear growth stage in such a way as to keep step with the zonal phase propagation of background IGW.

Eigenmodes represent the optimum growth over an infinite, as opposed to finite, time. In reality, the initial noise spectrum has finite amplitude, decreasing with horizontal wavenumber. The most relevant wavenumber corresponds to the value of k for which instability (modal or nonmodal) produces large perturbations in the least amount of time. Consider the growth of eigenmodes on a background spectrum such that

$$E(k, t) = E_0\left(\frac{k}{k_0}\right)^{-p} \exp \omega_i(k)t. \tag{4.1}$$

The time required for any spectral component to reach E_0 is

$$\tau(k) = \frac{p \ln(k/k_0)}{\omega_i(k)}, \tag{4.2}$$

having a minimum at some $k < k_m$ (unless the initial noise is white, i.e., $p = 0$). Convection, therefore, should display zonal scale selection without numerical hyperdiffusion if $p \neq 0$. This somewhat unrealistic example assumes that eigenmodes have maximum growth for any optimization interval but serves to illustrate the point that a most unstable eigenmode at $k = k_m$ (or the saddle point of absolute instability) is not necessarily the most relevant instability in a particular situation.

Nonmodal and/or absolute instabilities may prove important for saturation of IGW via shear instability along the curve $a = a_s(R)$ defined in (1.2). Results of Fritts and Yuan (1989) and those of section 3 demonstrate that as a is increased, eigenmodes of shear instability in the steady, parallel-flow approximation become important a finite distance above this curve, along some other curve $a = a_n(R, \alpha)$. For subcritical a, this curve begins at a point near $(R, a) = (0.7, 1)$ and extends to lower a as R is increased, roughly in parallel to the curve defined by (1.2).

5. Conclusions

Local shear and convective instabilities of internal inertia-gravity waves (IGW) were examined assuming a steady, plane-parallel flow with vertical profiles of horizontal velocity and static stability resembling an IGW packet in a basic state at rest, without mean vertical shear. The eigenproblem can be described in terms of a nondimensional rotation rate $R = f/\hat{\omega}_0 < 1$, where f is the Coriolis parameter, $\hat{\omega}_0$ is IGW intrinsic frequency, and IGW amplitude a, such that $a = 1$ for convectively neutral waves. In the nonrotating case, shear instability is possible only for convectively supercritical waves, with horizontal wavevector aligned parallel or nearly parallel to the plane of IGW propagation. Transverse convection, with wavevector aligned perpendicular to the plane of IGW propagation, displays faster growth than parallel shear or convective instability at any horizontal wavenumber. For intermediate R, eigenmodes in supercritical IGW are characterized at small horizontal wavenumber k by a transverse mode of convective instability and a parallel mode of shear instability. The transverse mode again has larger growth rate at small k but is suppressed at high wavenumbers where parallel convection prevails. Shear production of perturbation kinetic energy in transverse instability is positive (negative) at intermediate or large (small) R. For R approaching unity, shear instability takes precedence over convective instability at all azimuths regardless of a. In this limit, growth of the most unstable mode is almost independent of azimuth. It is shown that the parallel (symmetric and antisymmetric) shear instabilities of an

IGW are analogous to the unstable sinuous and varicose modes of a stratified jet. The presence of two instability critical levels in the zonal direction evidently enhances growth of the symmetric mode, making it competitive with transverse shear instability at large *R.*

Effects of a mean shear were discussed briefly, and the stability problem of an earlier two-dimensional (nonrotating) simulation (Dunkerton and Robins 1992) was revisited, considering eigenmode trajectories in more detail and examining the growth of transverse convection. It was shown that negative static stability at the center of DR's wave packet is not essential for growth of the parallel eigenmode. As in the simpler problem without mean shear, transverse convection is preferred at any *k.* Whether the transverse component of instability would actually be important in a 3D simulation of DR's wave packet depends on the initial noise spectrum. With isotropic initial noise of moderate amplitude, the stability analysis suggests that transverse convection will dominate. With very small initial noise (such that the zonal wavenumber spectrum is filled by self-interaction of the primary wave) parallel shear instability will prevail, at least initially. A combination of parallel shear instability and transverse convection may be the rule in these situations (Fritts et al. 1994; Winters and Riley 1992; Winters and d'Asaro 1994). Unless the growth rate of competing modes is nearly equal, however, one mode will emerge at finite amplitude prior to the others, assuming similar initial amplitudes. As soon as one mode attains finite amplitude, the ''basic state'' is altered from that of a pure IGW. Additional unstable modes may continue to develop, but their growth rate and structure will be significantly different from those implied by a linear stability analysis. Interesting situations can arise in breaking IGW as a result, for example, secondary convective instabilities within localized KH billows or (as suggested by a reviewer) secondary shear instabilities driven by local stretching and thinning of vorticity due to counterrotating convective rolls.

The nonlinear breakdown of inertia-gravity waves was investigated recently by LD97a,b in a 3D numerical model, confirming the stability analysis at large *R,* including a weak azimuthal dependence of shear instability and prevalence of shear over convective instability. With adequate spatial resolution, numerical models enable us to investigate the mixing efficiency of breaking IGW. The importance of shear instability to vertical mixing in the atmosphere and ocean is that the unstable eigenmodes of shear instability and resulting finite-amplitude billows overlap the convectively *stable* part of the wave field and thereby cause potentially greater mixing than would otherwise be possible in convectively unstable waves.

Acknowledgments. Discussions with Dave Fritts and Pascale Lelong are gratefully acknowledged. This research was supported by the National Science Foundation, Grants ATM-9123797 and ATM-9500613, and the Air Force Office of Scientific Research, Contract F49620-92-C-0033.

REFERENCES

Barat, J., 1983: The fine structure of the stratospheric flow revealed by differential sounding. *J. Geophys. Res.,* **88,** 5219–5228.

Clark, P. D., and P. H. Haynes, 1996: Inertial instability on an asymmetric low-latitude flow. *Quart. J. Roy. Meteor. Soc.,* **122,** 151–182.

Coy, L., and D. C. Fritts, 1988: Gravity wave heat fluxes: A Lagrangian approach. *J. Atmos. Sci.,* **45,** 1770–1780.

Delisi, D. P., and T. J. Dunkerton, 1989: Laboratory observations of gravity wave critical-layer flows. *Pure Appl. Geophys.,* **130,** 445–461.

Dunkerton, T. J., 1982: Wave transience in a compressible atmosphere. Part III: The saturation of internal gravity waves in the mesosphere. *J. Atmos. Sci.,* **39,** 1042–1051.

——, 1984: Inertia–gravity waves in the stratosphere. *J. Atmos. Sci.,* **41,** 3396–3404.

——, 1989: Theory of internal gravity wave saturation. *Pure Appl. Geophys.,* **130,** 373–397.

——, 1990: Eigenfrequencies and horizontal structure of divergent barotropic instability originating in tropical latitudes. *J. Atmos. Sci.,* **47,** 1288–1301.

——, 1993: Inertial instability of nonparallel flow on an equatorial β-plane. *J. Atmos. Sci.,* **50,** 2744–2758.

——, and R. E. Robins, 1992: Radiating and nonradiating modes of secondary instability in a gravity wave critical layer. *J. Atmos. Sci.,* **49,** 2546–2559.

Fritts, D. C., 1984: Gravity wave saturation in the middle atmosphere: A review of theory and observations. *Rev. Geophys. Space Phys.,* **22,** 275–308.

——, and T. J. Dunkerton, 1985: Fluxes of heat and constituents due to convectively unstable gravity waves. *J. Atmos. Sci.,* **42,** 549–556.

——, and P. K. Rastogi, 1985: Convective and dynamical instabilities due to gravity wave motions in the lower and middle atmosphere: Theory and observations. *Radio Sci.,* **20,** 1247–1277.

——, and L. Yuan, 1989: Stability analysis of inertio-gravity wave structure in the middle atmosphere. *J. Atmos. Sci.,* **46,** 1738–1745.

——, J. R. Isler, and O. Andreassen, 1994: Gravity wave breaking in two and three dimensions. 2: Three-dimensional evolution and instability structure. *J. Geophys. Res.,* **99,** 8109–8124.

Hazel, P., 1972: Numerical studies of the stability of inviscid stratified shear flows. *J. Fluid Mech.,* **51,** 39–61.

Huerre, P., and P. A. Monkewitz, 1990: Local and global instabilities in spatially developing flows. *Annu. Rev. Fluid Mech.,* **22,** 473–537.

Klostermeyer, J., 1991: Two- and three-dimensional parametric instabilities in finite-amplitude internal gravity waves. *Geophys. Astrophys. Fluid Dyn.,* **61,** 1–25.

Koop, C. G., and B. McGee, 1986: Measurements of internal gravity waves in a continuously stratified shear flow. *J. Fluid Mech.,* **172,** 453–480.

Lindzen, R. S., 1981: Turbulence and stress due to gravity wave and tidal breakdown. *J. Geophys. Res.,* **86C,** 9707–9714.

——, B. Farrell, and K.-K. Tung, 1980: The concept of wave overreflection and its application to baroclinic instability. *J. Atmos. Sci.,* **37,** 44–63.

Lombard, P. N., 1994: The stability of finite amplitude internal gravity waves. Ph.D. thesis, University of Washington, 162 pp.

McComas, C. H., and F. P. Bretherton, 1977: Resonant interaction of oceanic internal waves. *J. Geophys. Res.,* **82,** 1397–1412.

Pierrehumbert, R. T., 1984: Local and global baroclinic instability of zonally varying flow. *J. Atmos. Sci.,* **41,** 2141–2162.

Sutherland, B. R., and W. R. Peltier, 1994: Turbulence transition and

internal wave generation in density stratified jets. *Phys. Fluids,* **6,** 1267–1284.

Walterscheid, R. L., and G. Schubert, 1990: Nonlinear evolution of an upward propagating gravity wave: Overturning, convection, transience, and turbulence. *J. Atmos. Sci.,* **47,** 101–125.

Winters, K. B., and E. A. D'Asaro, 1989: Two-dimensional instability of finite amplitude internal gravity wave packets near a critical level. *J. Geophys. Res.,* **94,** 12 709–12 719.

——, and J. J. Riley, 1992: Instability of internal waves near a critical level. *Dyn. Atmos. Ocean,* **16,** 249–278.

——, and E. A. D'Asaro, 1994: Three-dimensional wave instability near a critical level. *J. Fluid Mech.,* **272,** 255–284.

Yamanaka, M. D., and H. Tanaka, 1984: Propagation and breakdown of internal inertio-gravity waves near critical levels in the middle atmosphere. *J. Meteor. Soc. Japan,* **62,** 1–16.

Yuan, L., and D. C. Fritts, 1989: Influence of a mean shear on the dynamical instability of an inertia-gravity wave. *J. Atmos. Sci.,* **46,** 2562–2568.